Letters 10, 62 (1967).
[22]M. DiDomenico, Jr., and S. H. Wemple, J. Appl. Phys. 40, 720 (1969).
[23]R. C. Miller and W. A. Nordland, Appl. Phys. Letters 16, 174 (1970).
[24]J. Jerphagnon, Appl. Phys. Letters 16, 298 (1970).
[25]C. R. Jeggo and G. D. Boyd, J. Appl. Phys. (to be published).
[26]R. C. Miller, in Proceedings of the Second International Meeting on Ferroelectricity, Tokyo, 1969 (unpublished).
[27]T. Ogawa, J. Phys. Soc. Japan 25, 1126 (1968).
[28]S. C. Abrahams and J. L. Bernstein, Acta Cryst. 25, 1233 (1969).
[29]V. S. Suvorov and A. S. Sonin, Zh. Eksperim. i Teor. Fiz. 54, 1044 (1968) [Soviet Phys. JETP 27, 557 (1968)].
[30]D. A. Kleinman (unpublished).
[31]S. C. Abrahams, S. K. Kurtz, and P. B. Jamieson, Phys. Rev. 172, 551 (1968).
[32]The treatment given in Ref. 25 relates also nonlinear coefficients and crystallographic structure; it leads to results taking into account both vector and septor parts. The interest of Eq. (34) lies in the possibility of a quick evaluation for Δz.
[33]R. C. Miller and W. A. Nordland, Optics Commun. 1, 400 (1970).
[34]R. C. Miller and W. A. Nordland (unpublished).
[35]K. F. Hulme, P. H. Davies, and V. M. Cound, J. Phys. C 2, 855 (1969).

PHYSICAL REVIEW B VOLUME 2, NUMBER 4 15 AUGUST 1970

Ultrasonic Beam Mixing as a Measure of the Nonlinear Parameters of Fused Silica and Single-Crystal NaCl†*

Russel W. Dunham‡ and Hillard B. Huntington
Department of Physics and Astronomy, Rensselaer Polytechnic Institute, Troy, New York 12181
(Received 3 February 1970)

The mixing action of two crossed ultrasonic beams has been studied. The theoretical treatment of Taylor and Rollins is extended to include the all-pure-mode cases for the prosess

$$L(\omega_1) - T\begin{Bmatrix}\omega_2\\ \omega_1-\omega_2\end{Bmatrix} \rightarrow T\begin{Bmatrix}\omega_1-\omega_2\\ \omega_2\end{Bmatrix}$$

in cubic single crystals. Five such cases exist in cubic crystals; two in the (001) mixing plane and with $L(\omega_1)$ propagated in either of two fixed directions [100] and [110]; and the other three in the $(1\bar{1}0)$ mixing plane and with $L(\omega_1)$ propagated in any of three fixed directions [110], [111], and [001]. The transverse waves are polarized normal to the mixing plane in all five cases and propagate in directions within the plane corresponding to the selection rules on frequency and propagation vector. The conversion efficiency was measured over a range of input frequency ratios, $a=\omega_2/\omega_1$ for the two independent transverse-polarization states for the above process in fused silica and for the two pure-mode cases in the (001) plane in NaCl. A comparison technique using the interchange equivalence of $T(\omega_2)$ and $T(\omega_1-\omega_2)$ effectively eliminated the transducer-bond efficiencies. These measurements were used to determine two of the three independent third-order elastic constants of fused silica. In the case of NaCl, the two ratios of linear combinations of second- and third-order elastic constants corresponding to the two (001)-plane pure-mode cases were determined. The above comparison technique was not applied to the other three pure-mode cases because the transverse anisotropy in the $(1\bar{1}0)$ plane leads to refractive effects on the transverse beams that render the technique inapplicable.

I. INTRODUCTION

In this investigation we explore the mixing action in the crossing of ultrasonic beams and the measurement of the conversion efficiency to determine parameters characterizing the nonlinearity of materials. When two large-amplitude ultrasonic waves intersect in a solid at an angle appropriate to the particular ratio of their frequencies, a third ultrasonic wave generally radiates from their common volume of intersection. The third wave propagates in still another direction so that there is a conservation relation among the three propagation vectors involved. The third wave has either the sum or difference frequency of the two primary waves depending on the particular mode combination.

Rollins, Taylor, and Todd[1] were first to make a qualitative experimental study of these interactions between ultrasonic waves followed at a later date by Krasilnikov and Zarembo.[2] Jones and Kobett[3] had previously carried out a classical wave analysis for the wave mixing processes in isotropic solids. Taylor and Rollins[4] later obtained the same results through a semiquantum-mechanical approach.

The present work is concerned with primarily two developments: (i) extension of the theoretical approach of Taylor and Rollins to include interactions in cubic crystals, and (ii) a more quantitative experimental study of both isotropic solids and cubic crystals to obtain information on the nonlinear parameters involved.

II. GENERAL THEORETICAL CONSIDERATIONS

Most of what is included here is repetitious of the general semiquantum-mechanical approach as outlined by Taylor and Rollins[4] and is included as a review.

The deformation of an elastic medium is completely characterized by the components η_{ij} of the deformation tensor:

$$\eta_{ij}=\frac{1}{2}\left(\frac{\partial U_i}{\partial x_i}+\frac{\partial U_j}{\partial x^i}+\frac{\partial U^k}{\partial x^i}\frac{\partial U_k}{\partial x^j}\right) , \tag{1}$$

where the U_i are the components of the displacement vector for a point in the medium and the x^i are the initial coordinates of the point. The deformation energy density $\mathcal{E}$ is expressed as a Taylor series expansion in the η_{ij}, retaining only terms through third order in the deformation tensor components. After the terms in $\mathcal{E}$ are effectively reordered according to order in the displacement gradient components $\partial U_i/\partial x^j$, the collection of terms of second order in the $\partial U_i/\partial x^j$ is taken as the "unperturbed" part of $\mathcal{E}$ and, correspondingly, the collection of terms of third order in the $\partial U_i/\partial x^j$ is taken as the "perturbation energy density." Note that it is the terms of higher order with respect to $\partial U_i/\partial x^j$ that give rise to nonlinear effects. This becomes more evident once the $\partial U_i/\partial x^j$ are "quantized" by writing them as an appropriate combination of the creation and annihilation operators:

$$\frac{\partial U_i}{\partial x^j}=ie_ik_j\,(ae^{i\vec{k}\cdot\vec{r}}+a^*e^{-i\vec{k}\cdot\vec{r}}) . \tag{2}$$

Here e_i are the components of the unit polarization vector k_i the components of the propagation vector, and a^* and a, respectively, the creation and annihilation operators of the linear harmonic oscillator. Examining Eq. (1), which is derived from purely geometrical arguments, reveals that η_{ij} has a term already quadratic in the $\partial U_i/\partial x^j$. Hence, nonlinear phenomena have two fundamental sources: (a) an intrinsic geometrical contribution arising from the form of η_{ij} and (b) physical contributions arising from the nature of the effective interatomic force field.

Once the perturbation energy is obtained, then the standard techniques of time-dependent perturbation theory can be applied to calculate the transition rate for the mixing process. This requires visualizing the two intersecting beams as ideally dense homogeneous beams of "phonons." This is where, as was pointed out by Barrett and Matsinger,[5] the procedure fails to be rigorously quantum mechanical. The results, however, are in agreement with the classical wave treatment.

The transition rate gives the rate of creation of "phonons" in the new third mode. The results are written in terms of the displacement amplitudes of the three waves by equating the classical energy density for an ultrasonic beam to $\eta\hbar\omega$, where η is the phonon density in the beam, ω is its angular frequency, and $\hbar$ is Planck's constant divided by 2π. From this it can be seen that it is the rms displacement amplitudes that appear in the final expression.

III. THEORY: ISOTROPIC SOLIDS AND SINGLE CRYSTALS

The theoretical procedure outlined above was applied to isotropic solids by Taylor and Rollins.[4] Only the results will be repeated here for the interaction

$$L(\omega_1)-T(\omega_2)\rightarrow T(\omega_1-\omega_2) .$$

The displacement amplitude X_3 of the interaction wave $T(\omega_1-\omega_2)$ is given in terms of the displacement amplitudes X_1 and X_2, respectively, for the input longitudinal wave $L(\omega_1)$ and the input transverse wave $T(\omega_2)$ by

$$X_3=X_1X_2\,(V\omega_1^3/8\pi r\rho c_t^4c_l)\,D\Gamma(a) . \tag{3}$$

In this expression, V is the common volume of intersection of the two input beams, ω_1 is the angular frequency of the input longitudinal beam, r is the distance from the center of V to the receiving transducer, ρ is the material mass density, and c_t and c_l, respectively, are the transverse and longitudinal velocities of propagation in the material. The factor D represents a linear combination of second- and third-order elastic constants and depends on the polarization of the two transverse modes. The remaining factor $\Gamma(a)$ is a function of the input frequency ratio $a=\omega_2/\omega_1$, the form of which also depends on the polarization of the transverse waves. Two independent polarization states exist in isotropic materials for the class of inter-

actions $L \rightarrow T+T$. One has the polarization of the two transverse waves parallel to the plane of interaction, whereas the other involves transverse waves polarized perpendicular to the plane of interaction. The explicit form of $D\Gamma(a)$ for these two polarization states is given in Table I for the interaction case

$$L(\omega_1) - T(\omega_2) \rightarrow T(\omega_1 - \omega_2) ,$$

along with expressions for the angles ϕ and γ between $L(\omega_1)$ and $T(\omega_2)$ and between $L(\omega_1)$ and $T(\omega_1 - \omega_2)$, respectively. The angles are uniquely determined by the selection rules on the propagation vectors and the frequencies. The constants A, B, C, λ, and μ appearing in the table are defined as the coefficients in the expansion of the strain energy density to third order in the invariants of strain as follows[4]:

$$E = \tfrac{1}{2}\lambda(I_1)^2 + \mu I_2 + \tfrac{1}{3}AI_3 + BI_1I_2 + \tfrac{1}{3}C(I_1)^3 . \quad (4)$$

The first-, second-, and third-order invariants of strain, I_1, I_2, and I_3, respectively, are

$$I_1 \equiv \eta_k^k, \quad I_2 \equiv \eta_i^k \eta_k^i, \quad I_3 \equiv \eta_i^k \eta_m^i \eta_k^m . \quad (5)$$

Cases involving polarizations that are intermediate between these two cases are described by replacing $D\Gamma(a)$ by the following linear combination of $D_{\parallel}\Gamma_{\parallel}(a)$ and $D_{\perp}\Gamma_{\perp}(a)$:

$$D\Gamma(a) = [\sin\theta_2 \sin\theta_3 D_{\perp}\Gamma_{\perp}(a) + \cos\theta_2 \cos\theta_3 D_{\parallel}\Gamma_{\parallel}(a)] . \quad (6)$$

The angles θ_2 and θ_3 are those, respectively, between the input and interaction transverse polarization vectors and the interaction plane.

In cubic single crystals, several complications arise. The anisotropy gives rise to impure modes and to the deviation of Poyntings vector from the propagation direction. The latter is probably the more severe limitation on the experimental technique presently employed. It is desirable to treat only cases with all modes remaining pure over the entire allowed band of input frequency ratios. Analysis of the eigenvalue-eigenvector problem for an elastic wave propagating through a cubic single crystal reveals that five such pure-mode cases exist for the interaction $L(\omega_1) - T(\omega_2) \rightarrow T(\omega_1 - \omega_2)$. Two of these cases occur with the (001) plane as the plane of interaction and have the longitudinal wave propagating down either the [100] axis or the [110] axis. The remaining three take place in the $(1\bar{1}0)$ plane with $L(\omega_1)$ propagating down any one of the three axes [110], [111], and [001]. The two transverse waves are polarized normal to the plane of interaction in all five cases. Note that in each case the longitudinal wave is propagated in a fixed direction whereas the transverse waves, which remain pure for arbitrary propagation directions within the respective interaction planes, propagate in directions that correspond to the conservation conditions on the propagation vectors and the frequencies. Thus, the propagation direction for the transverse waves varies with the input frequency ratio.

The displacement amplitude of the interaction wave is obtained in a manner analogous to that for an isotropic material. The strain energy density $\mathcal{E}$ in this case has the following form[6]:

$$\mathcal{E} = \tfrac{1}{2}c_{11}(\eta_{11}^2 + \eta_{22}^2 + \eta_{33}^2) + c_{12}(\eta_{11}\eta_{22} + \eta_{22}\eta_{33} + \eta_{33}\eta_{11}) + 2c_{44}(\eta_{12}^2 + \eta_{23}^2 + \eta_{31}^2) + \tfrac{1}{6}C_{111}(\eta_{11}^3 + \eta_{22}^3 + \eta_{33}^3)$$
$$+ \tfrac{1}{2}C_{112}[\eta_{11}^2(\eta_{22} + \eta_{33}) + \eta_{22}^2(\eta_{33} + \eta_{11}) + \eta_{33}^2(\eta_{11} + \eta_{22})] + C_{123}\eta_{11}\eta_{22}\eta_{33} + 8C_{456}\eta_{12}\eta_{23}\eta_{31}$$
$$+ 2C_{144}(\eta_{11}\eta_{23}^2 + \eta_{22}\eta_{31}^2 + \eta_{33}\eta_{12}^2) + 2C_{166}[\eta_{12}^2(\eta_{11} + \eta_{22}) + \eta_{23}^2(\eta_{22} + \eta_{33}) + \eta_{31}^2(\eta_{33} + \eta_{11})] . \quad (7)$$

The third-order eleastic constants C_{ijk} are in Brugger's definition.[7] The η_{ij} are the usual Lagrangian strain parameters previously defined.

Upon rewriting $\mathcal{E}$ in terms of the symmetric and antisymmetric parts of the displacement gradient $\partial U_i/\partial \delta_i$, namely, ϵ_{ij} and ω_{ij}, respectively, and regrouping the terms according to order in the ϵ_{ij} and ω_{ij}, one obtains the following form:

$$\mathcal{E} = \mathcal{E}_0 + \mathcal{E}' . \quad (8)$$

TABLE I. $D\Gamma(a)$ for the two independent polarization cases in isotropic materials. $\cos\phi = 1/c - (1-c^2)/2ac$, $\tan\gamma = (a\sin\phi)/(a\cos\phi - c)$.

T-polarized normal to mixing plane $D_{\perp}\Gamma_{\perp}(a)$	T-polarized parallel to mixing plane $D_{\parallel}\Gamma_{\parallel}(a)$
$\tfrac{1}{2}a[(A+4\mu)(c - a\cos\phi)\cos\phi + 2(B+\lambda)(c\cos\phi - a)]$	$[a/2(1-a)][2(2B+A+\lambda+3\mu)(c\cos\phi - a)^2 - (2B+A+2\mu)(1-a)^2]$

The first term $\mathcal{E}_0$ represents the collection of second-order terms in the ϵ_{ij}, and the second term $\mathcal{E}'$ represents the collection of terms of third order in the ϵ_{ij} and ω_{ij}. The terms in $\mathcal{E}_0$ represent, in perturbation theory, the unperturbed part of the strain energy density, whereas $\mathcal{E}'$ represents the perturbation energy density. In infinitesimal elastic theory, the terms contained in $\mathcal{E}'$ are the ones that are neglected. The explicit forms of $\mathcal{E}_0$ and $\mathcal{E}'$ are

$$\mathcal{E}_0=\tfrac{1}{2}c_{11}(\epsilon_{11}^2+\epsilon_{22}^2+\epsilon_{33}^2)+c_{12}(\epsilon_{11}\epsilon_{22}+\epsilon_{22}\epsilon_{33}+\epsilon_{33}\epsilon_{11})+2c_{44}(\epsilon_{12}^2+\epsilon_{23}^2+\epsilon_{31}^2)\quad, \tag{9}$$

$$\begin{aligned}\mathcal{E}'=&\tfrac{1}{2}c_{11}(\epsilon_k^k\omega_m^l\omega_l^m+2\epsilon_k^k\epsilon_m^l\omega_l^m)+\tfrac{1}{2}c_{12}[\epsilon_{11}(\omega_{k2}\omega_2^k+\omega_{k3}\omega_3^k)+\epsilon_{22}(\omega_{k1}\omega_1^k+\omega_{k3}\omega_3^k)\\&+\epsilon_{33}(\omega_{k2}\omega_2^k+\omega_{k1}\omega_1^k)+2\epsilon_{11}(\epsilon_{k2}\omega_2^k+\epsilon_{k3}\omega_3^k)+2\epsilon_{22}(\epsilon_{k1}\omega_1^k+\epsilon_{k3}\omega_3^k)+2\epsilon_{33}(\epsilon_{k2}\omega_2^k+\epsilon_{k1}\omega_1^k)]\\&+2c_{44}[\epsilon_{12}\omega_{k1}\omega_2^k+\epsilon_{23}\omega_{k2}\omega_3^k+\epsilon_{31}\omega_{k3}\omega_1^k+\epsilon_{12}(\epsilon_{k1}\omega_2^k+\epsilon_{k2}\omega_1^k)+\epsilon_{23}(\epsilon_{k2}\omega_3^k+\epsilon_{k3}\omega_2^k)\\&+\epsilon_{31}(\epsilon_{k3}\omega_1^k+\epsilon_{k1}\omega_3^k)]+\tfrac{1}{6}(C_{111}+3c_{11})(\epsilon_{11}^3+\epsilon_{22}^3+\epsilon_{33}^3)+\tfrac{1}{2}(C_{112}+c_{12})[\epsilon_{11}^2(\epsilon_{22}+\epsilon_{33})+\epsilon_{22}^2(\epsilon_{11}+\epsilon_{33})+\epsilon_{33}^2(\epsilon_{11}+\epsilon_{22})]\\&+C_{123}\epsilon_{11}\epsilon_{22}\epsilon_{33}+(8C_{456}+6c_{44})\epsilon_{12}\epsilon_{23}\epsilon_{31}+(2C_{144}+c_{12})(\epsilon_{11}\epsilon_{23}^2+\epsilon_{22}\epsilon_{31}^2+\epsilon_{33}\epsilon_{12}^2)+\tfrac{1}{2}(4C_{166}+c_{11}+c_{12}+4c_{44})\\&\times[\epsilon_{12}^2(\epsilon_{11}+\epsilon_{22})+\epsilon_{23}^2(\epsilon_{22}+\epsilon_{33})+\epsilon_{31}^2(\epsilon_{31}^2(\epsilon_{33}+\epsilon_{11})]\,.\end{aligned} \tag{10}$$

Next, the displacement amplitudes are written, assuming plane waves, in the quantum representation in a manner corresponding to Eq. (2),

$$\vec{u}^{(n)}(\vec{r})=\hat{e}^{(n)}(a^{(n)}e^{i\vec{k}^{(n)}\cdot\vec{r}}+a^{(n)*}e^{-i\vec{k}^{(n)}\cdot\vec{r}})\,, \tag{11}$$

with $a^{(n)*}$ and $a^{(n)}$ as the creation and annihilation operators for the linear harmonic oscillator. Then, the total displacement vector field for the problem is taken as the sum of the fields of the two primary waves and the assumed third interaction wave:

$$\vec{u}(\vec{r})=\sum_{n=1}^{3}\vec{u}^{(n)}(\vec{r})\,. \tag{12}$$

Equation (11) is used to calculate ϵ_{ij} and ω_{ij} explicitly in terms of the creation and annihilation operators, and then Eq. (12) implies that

$$\epsilon_{ij}=\sum_{n=1}^{3}\epsilon_{ij}^{(n)}\quad\text{and}\quad\omega_{ij}=\sum_{n=1}^{3}\omega_{ij}^{(n)}\,.$$

The bracketed superscript n numbers the three ultrasonic waves. The convention will be to take $n=1$ as $L(\omega_1)$, $n=2$ as $T(\omega_2)$, and $n=3$ as $T(\omega_1-\omega_2)$.

The Golden Rule of time-dependent perturbation theory can now be used to calculate the transition rate for the mixing process described above. This rule gives the transition rate as

$$R=2\pi/\hbar\,|\langle f|H'|i\rangle|^2\mathfrak{D}_f(\mathcal{E}_i), \tag{13}$$

where $\mathcal{E}_i$ is the energy of the initial state and $\mathfrak{D}_f(\mathcal{E}_i)$ is the density of final states about $\mathcal{E}_i$. H' is the perturbation energy and is given by

$$H'=\int_V\mathcal{E}'\,d\tau\,. \tag{14}$$

The volume integral extends over the common volume of intersection for the two input beams. The initial- and final-state vectors are given, respectively, by

$$\begin{aligned}&\text{and}\quad|i\rangle=|N_1\rangle\,|N_2\rangle\,|0\rangle\,,\\&\qquad|f\rangle=|N_1-1\rangle\,|N_2+1\rangle\,|1\rangle,\end{aligned} \tag{15}$$

in which N_1 and N_2 are the initial numbers of phonons in beams 1 and 2, respectively.

When this calculation is carried through, Eq. (3) is again obtained relating the displacement amplitudes. The form of $\Gamma(a)$ for the five cases is

$$\Gamma(a)=(c-a\cos\phi)\,a\cos\phi-\delta a^2\sin^2\phi-\epsilon a\sin\phi\,(c-2a\cos\phi). \tag{16}$$

The parameters δ and ϵ are given in Tables II and III for the five pure-mode cases.

It should be pointed out that, while there is transverse isotropy for the cases in the (001) plane, the transverse velocity in the $(1\bar{1}0)$ plane depends on the direction of propagation in this plane. Hence, the Poynting's vector $\vec{P}$ for the transverse waves involved in the three pure-mode cases in the $(1\bar{1}0)$ plane deviates from the propagation vector $\vec{k}$ by as much as 10° in NaCl. The angle of deviation β of $\vec{P}$ from $\vec{k}$ is a function of orientation angle θ between k and the [110] axis in NaCl, as shown in Fig. 1. Because of this complication, the present

TABLE II. Conversion parameters δ and ϵ for $L(\omega_1)-T(\omega_2)\rightarrow T(\omega_1-\omega_2)$ in the (001) plane in cubic materials. All three waves are pure modes.

$L(\omega_1)$ Propagation direction	δ	ϵ
[100]	$\dfrac{(c_{12}+C_{144})}{(c_{11}+C_{166})}$	0
[110]	$\dfrac{(c_{11}+c_{12}-2c_{44}+C_{144}+C_{166}-2C_{456})}{(c_{11}+c_{12}+2c_{44}+C_{144}+C_{166}+2C_{456})}$	0

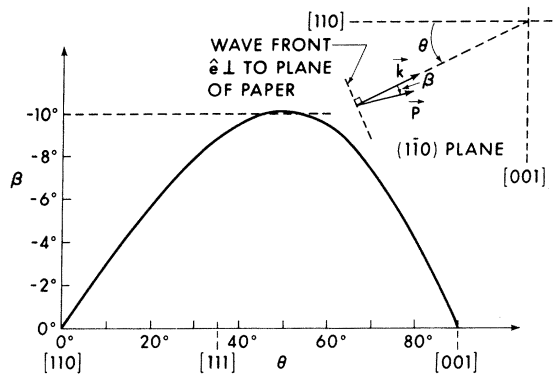

FIG. 1. Angle β between $\vec{P}$ and $\vec{k}$ as a function of the orientation angle θ between $\vec{k}$ and the [110] axis for the pure transverse mode in the (1$\bar{1}$0) plane for NaCl.

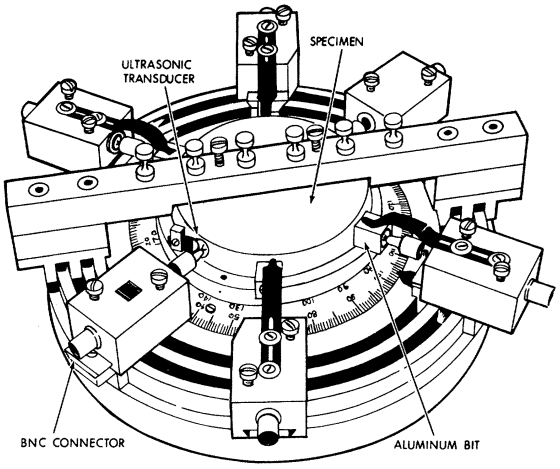

FIG. 2. Ultrasonic goniometer.

experimental technique was applied only to the two cases in the (001) plane. [8]

IV. EXPERIMENTAL ARRANGEMENT AND TECHNIQUE

The specimens were 4-in. -diam, $\frac{1}{2}$-in. -thick disk-shaped blanks of G. E. Type 151 fused silica and Harshaw optical single-crystal NaCl oriented with the plane of the disk in a (100) plane. An ultrasonic "goniometer," shown in Fig. 2, was designed and constructed to hold the disk specimen and provide electrical contacts to all transducers over a wide range of angles. This device also doubled as a multibonding clamp.

The two input transducers, X-cut quartz for $L(\omega_1)$ and Y-cut quartz for $T(\omega_2)$. were excited by rf pulses from two Arenberg model PG650C high-power rf pulse generators. The output impedance of these generators is 93 Ω, whereas typical transducer operating impedances are on the order of 100 kΩ. Hence, simple tuned transformers were inserted for better impedance matching. Tuning in the secondary circuit of these transformers allowed tuning out of the transducer shunt capacitance. These transformers reduced the insertion loss by as much as 40 dB in some cases.

The interaction signal $T(\omega_1 - \omega_2)$, which was picked up by another Y-cut transducer, was observed using an Arenberg model PA-620-B preamplifier placed immediately after the transducer. The preamplifier provided a selection of slug tuned coils to resonate with the transducer capacitance. Its bandwidth was narrow enough to exclude extraneous signals from the primary beams, provided the input frequency ratio $a = \omega_2/\omega_1$ was not too close to $\frac{1}{2}$. The rf signal was then amplified further with an Arenberg model WA600E wide-band amplifier and displayed as a video signal on a cathode-ray oscilloscope.

Examination of the conversion efficiency $\Gamma(a)$ for both polarization cases in isotropic materials and the two cases in the (001) plane in cubic solids

TABLE III. Conversion parameters δ and ϵ for $L(\omega_1) - T(\omega_2) \rightarrow T(\omega_1 - \omega_2)$ in the (1$\bar{1}$0) plane in cubic materials. All three waves are pure modes.

$L(\omega_1)$ Propagation direction	δ	ϵ
[110]	$(2c_{12}+C_{144}+C_{166}-2C_{456})/[c_{11}+c_{12}+2c_{44}+\frac{1}{2}(C_{111}-C_{112})]$	0
[111]	$\left(\frac{3c_{11}+6c_{12}-6c_{44}+\frac{1}{2}(C_{111}-C_{123})+6C_{144}-4C_{456}}{3c_{11}+6c_{12}+12c_{44}+C_{111}-C_{123}-3C_{144}+6C_{166}-2C_{456}}\right)$	$\left(\frac{(\sqrt{\frac{1}{2}})(C_{111}-C_{123}+4C_{456}-6C_{166})}{3c_{11}+6c_{12}+12c_{44}+C_{111}-C_{123}-3C_{144}+6C_{166}-2C_{456}}\right)$
[001]	$(2c_{12}+C_{112}-C_{123})/2(c_{11}+C_{166})$	0

reveals that $\Gamma(a)$ is a function of the product $a(1-a)$ alone. Hence, $\Gamma(1-a)=\Gamma(a)$ for all values of $a=\omega_2/\omega_1$. Also, $\phi(1-a)=\gamma(a)$ and conversely, $\gamma(1-a)=\phi(a)$. These relations are merely a consequence of the fact that the interaction $L(\omega_1)-T(\omega_2)\rightarrow T(\omega_1-\omega_2)$ is analogous to stimulated emission. The primary transverse beam $T(\omega_2)$ acts as a stimulating field, when the angle ϕ is appropriate, to induce the longitudinal phonons to split into two transverse phonons, one enhancing the primary transverse beam $T(\omega_2)$, and the other $T(\omega_1-\omega_2)$ propagating at an angle γ with respect to the $L(\omega_1)$ beam. However, the process could have been stimulated by a $T(\omega_1-\omega_2)$ beam at the angle γ with respect to $L(\omega_1)$ to produce the interaction beam $T(\omega_2)$ at the angle ϕ with respect to $L(\omega_1)$. This equivalence can be applied to eliminate the proportionality factor between the displacement amplitude of an ultrasonic wave at the center of the disk specimen and the voltage produced on the receiving transducer. This proportionality factor, while constant for a given bonding, is not measurable with any degree of precision.

The arrangement shown in Fig. 3 illustrates the method used to get reliable data for the dependence of the conversion efficiency on the frequency ratio by a comparison method. In this figure, transducer 1 is an X-cut quartz transducer affixed to a flat on the edge of the disk specimen. It is used to generate the $L(\omega_1)$ pulse. The transducer 2 is Y-cut quartz mounted on a plano-concave aluminum bit machined to fit the edge of the disk. It is used to generate the transverse pulse $T(\omega_2)$. The transducer 3 is then used to observe the interaction signal $T(\omega_1-\omega_2)$, while the transducer 3′ is used to observe the straight through $T(\omega_2)$ pulse. The ratio of the voltage amplitude v_3 on transducer 3, which is receiving the interaction signal, to the voltage amplitude v_2 on transducer 2, which is receiving the primary signal, is related to the ratio of the corresponding displacement amplitudes X_3 and X_2 by

$$v_3/v_2=(K_3/K_2)X_3/X_2\ . \tag{17}$$

In this expression K_3 and K_2 are the respective proportionality constants.

For the complementary process, the transducer 2′ is used to send in a $T(\omega_1-\omega_2)$ pulse, which is observed on transducer 3, while the $L(\omega_1)$ pulse is still sent in through transducer 1. The interaction transverse signal $T(\omega_2)$ is observed with transducer 3′. The ratio of the voltage amplitude v_3', due to the interaction wave $T(\omega_2)$ and appearing on transducer 3′ to the voltage amplitude v_2', due to the straight through $T(\omega_1-\omega_2)$, is related to the ratio of the corresponding displacement amplitudes X_3' and X_2' by

$$v_3'/v_2'=(K_2/K_3)X_3'/X_2'\ . \tag{18}$$

Note that the same two proportionality constants K_2 and K_3 are involved but in a *reciprocal* fashion. These unknowns can be eliminated by taking the geometric mean in the following manner.

$$[(v_3/v_2)(v_3'/v_2')]^{1/2}=[(X_3/X_2)(X_3'/X_2')]^{1/2}\ . \tag{19}$$

Note that while the unprimed case refers to a frequency ratio $a=\omega_2/\omega_1$, the primed case corresponds to a frequency ratio $a'=(1-a)$. Hence,

$$\left[\left(\frac{v_3}{v_2}\right)\left(\frac{v_3'}{v_2'}\right)\right]^{1/2}=\left[\left(\frac{X_3}{X_2}\ \frac{X_3'}{X_2'}\right)\right]^{1/2}$$
$$=X_1\left(\frac{V_{\rm eff}(a)\omega_1^3}{8\pi r\rho c_t^4 c_l}\right)D\Gamma(a)\ . \tag{20}$$

The invariance $\Gamma(1-a)=\Gamma(a)$ was made use of in this result, and $V_{\rm eff}(a)\equiv[V(a)\,V(1-a)]^{1/2}$. The interaction volume $V(a)$ depends on a through the angle ϕ. It is taken as the common volume of intersection of two completely intersecting cylinders. The displacement amplitude X_1 and the angular frequency ω_1 of the $L(\omega_1)$ beam are assumed to remain constant.

Next, we define a quantity,

$$G_{\rm expt}(a)\equiv\left[\left(\frac{v_3}{v_2}\right)\left(\frac{v_3'}{v_2'}\right)\right]^{1/2}\Big/V_{\rm eff}(a)\ . \tag{21}$$

Then it becomes clear that $G_{\rm expt}(a)=\text{const}\times D\Gamma(a)$. Again it is assumed that X_1 and ω_1 are held constant. In the case of isotropic materials, two independent polarization states exist for the transverse waves, and, since by definition there is transverse degeneracy in isotropic solids, the angles ϕ and γ are independent of the polarization state. Hence, $V_{\rm eff}(a)$

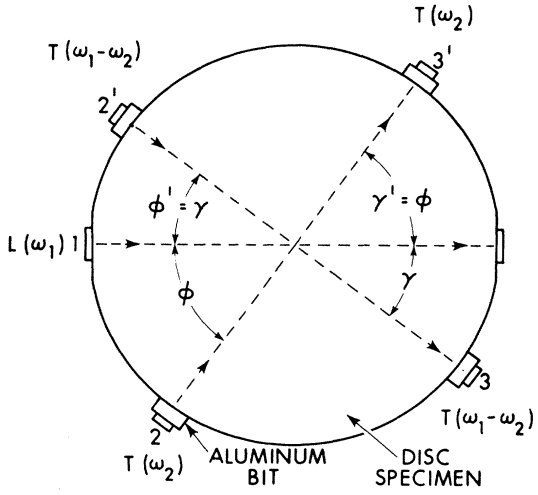

FIG. 3. Schematic of disk specimen with transducers in place.

is the same, at a given a, for both states of polarization and

$$\frac{G_{\text{expt}\,\parallel}(a)}{G_{\text{expt}\,\perp}(a)} = \frac{[(v_3/v_2)(v_3'/v_2')]_{\parallel}^{1/2}}{[(v_3/v_2)(v_3'/v_2')]_{\perp}^{1/2}} = \frac{D_{\parallel}\Gamma_{\parallel}(a)}{D_{\perp}\Gamma_{\perp}(a)} \equiv \sum(a; A, B) \ . \tag{22}$$

In this case, then, the measurements are made for each polarization state at selected values for the input frequency ratio $a = \omega_2/\omega_1$. The function $\sum(a; A, B)$ is fitted to this experimental data versus the frequency ratio a by varying A and B for the best fit.

For the two cases studied in NaCl, the procedure is necessarily a little different since there is only one pure-mode polarization state for each case. In these cases, a relative fit of $\Gamma(a)$ to $G_{\text{expt}}(a)$ was carried out by introducing the "renormalization" factor α. This was done by fitting the function $\alpha\Gamma(a; \delta)/\Gamma(a_0; \delta)$ to $G_{\text{expt}}(a)/G_{\text{expt}}(a_0)$ by varying α and δ. The data $G_{\text{expt}}(a)$ and the conversion efficiency $\Gamma(a; \delta)$ are normalized at some arbitrary measured frequency ratio a_0, as shown above. The best fit, however, may not correspond to the situation where the relative conversion efficiency passes through the data point at a_0. This constraint is relaxed by introducing the "renormalization" parameter α, as shown above. This parameter α has no physical significance but is introduced merely as an artifice to obtain the best relative fit. The conversion parameter δ is the quantity to be determined.

The geometric mean of the voltage ratios discussed, $[(v_3/v_2)(v_3'/v_2')]^{1/2}$, was measured using a calibration procedure illustrated in Fig. 4. The particular signal being received was observed with the connection schematically illustrated as "1" in the figure. The Arenberg preamplifier (APA) was tuned for peak video signal, which is observed on channel A of the cathode-ray oscilloscope (CRO). The gain of the Arenberg wide-band amplifier (AWBA) was adjusted to give a prescribed video voltage amplitude v_0 on the CRO. This video level was selected to be well below amplifier saturation and was chosen the same for all signals measured. The rf signal voltage amplitude v_n is related to v_0 by

$$v_0 = g_n v_n \ , \tag{23}$$

where g_n is the over-all gain of the preamplifier wide-band amplifier system.

Next, the connection schematically illustrated as "2" in Fig. 4 was used to get a relative calibration for the gain in the previous arrangement. The gain g_n is left unaltered and attenuator B is adjusted until the video voltage amplitude on the CRO is again v_0. This is necessary inasmuch as the system is nonlinear and g_n depends on the signal level. Furthermore, the frequency of the rf test signal being generated by the Arenberg pulse generator (APG) has been set precisely equal to that of the rf signal under study. The transducer simulator and decoupler serves the purpose of approximately simulating the impedance of the particular transducer involved in connection "1" and isolating the preamplifier from channel B of the CRO. This simulator introduces an attenuation factor α_n, which depends on the particular transducer being simulated. Hence, in this configuration, it is the net gain $\bar{g}_n$ that is measured:

$$\bar{g}_n = \alpha_n g_n \ . \tag{24}$$

The net gain $\bar{g}_n$ is measured by use of a dual-channel oscilloscope. The video signal is observed on channel A while the rf test signal into the transducer simulator is observed on channel B. With equal sensitivities in the two channels, the two traces are superimposed and attenuator A is adjusted to make the video signal just envelop the rf test signal. Then the net gain $\bar{g}_n$ can be read directly off attenuator A. The attenuation factor α_n remains unknown.

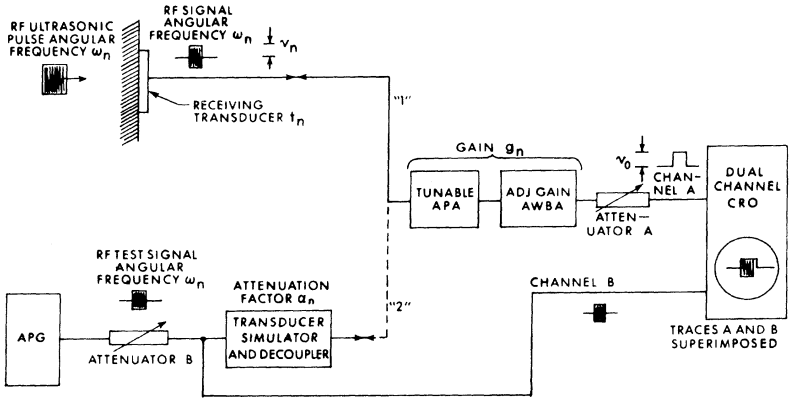

FIG. 4. Block diagram of arrangement for comparison calibration technique.

This procedure is applied to the method described in connection with Fig. 3. For the interaction signal $T(\omega_1 - \omega_2)$, we obtain, from Eqs. (23) and (24),

$$v_0 = g_3 v_3 \text{ and } \bar{g}_3 = \alpha_3 g_3 . \quad (25)$$

For the straight through transverse signal $T(\omega_2)$, we have

$$v_0 = g_2 v_2 \text{ and } \bar{g}_2 = \alpha_2 g_2 . \quad (26)$$

In the case of the complementary interaction, we get, for the interaction signal $T(\omega_2)$,

$$v_0 = g_3' v_3' \text{ and } \bar{g}_3' = \alpha_2 g_3' , \quad (27)$$

and for the straight through transverse signal $T(\omega_1 - \omega_2)$,

$$v_0 = g_2' v_2' \text{ and } \bar{g}_2' = \alpha_3 g_2' . \quad (28)$$

The following relations then result from Eqs. (25)–(28):

$$v_3/v_2 = g_2/g_3 , \quad v_3'/v_2' = g_2'/g_3' ,$$

$$\bar{g}_2/\bar{g}_3 = (\alpha_2/\alpha_3) g_2/g_3 = (\alpha_2/\alpha_3) v_3/v_2 ,$$

$$\text{and } \bar{g}_2'/\bar{g}_3' = (\alpha_3/\alpha_2) g_2'/g_3' = (\alpha_3/\alpha_2) v_3'/v_2' ; \quad (29)$$

hence,

$$[(v_3/v_2)(v_3'/v_2')]^{1/2} = [(\bar{g}_2/\bar{g}_3)(\bar{g}_2'/\bar{g}_3')]^{1/2} . \quad (30)$$

From Eq. (30) it can be seen that the experiment involves only the direct measurement of the four net gains $\bar{g}_2$, $\bar{g}_3$, $\bar{g}_2'$, and $\bar{g}_3'$. These gains were measurable to ± 1 dB.

V. EXPERIMENTAL RESULTS AND DISCUSSION

An oscilloscope display of the two impressed rf signals $T(\omega_2)$ and $L(\omega_1)$, and a typical rf interaction signal $T(\omega_1 - \omega_2)$ is shown in Fig. 5. The first pulse, labeled 2, is $T(\omega_2)$ with $f_2 = \omega_2/2\pi = 13.70$ MHz, while the second pulse, labeled 1, is $L(\omega_1)$ with $f_1 = \omega_1/2\pi = 31.14$ MHz. The third pulse, labeled 3, is the interaction signal $T(\omega_1 - \omega_2)$.

The fit of $\sum(a; A, B)$ to the data for fused silica was carried out by use of a general computer program for a maximum likelihood fit.[9] The results are shown in Fig. 6. The open circles are the data

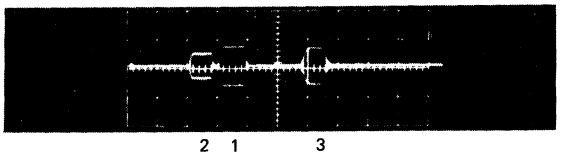

FIG. 5. Display of two impressed rf pulses and resulting rf interaction signal. Horizontal scale: 10 μsec/cm. Vertical scale: Arbitrary.

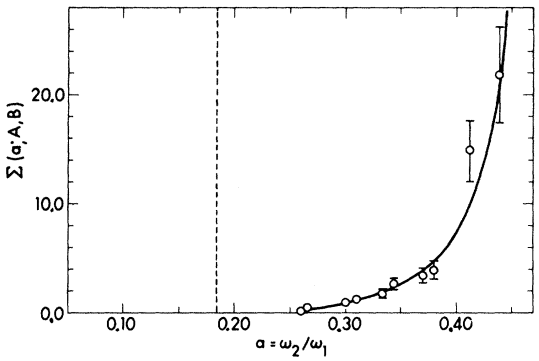

FIG. 6. Best fit of $\Sigma(a; A, B)$ to the experimental data (open circles) for G. E. Type 151 fused silica.

points and solid curve is $\sum(a; A, B)$ for the best fit. The values of A and B for the best fit above, along with those determined by Bogardus[10] using the velocity versus stress method, are presented in Table IV. Note that while there is good agreement for the constant A, the constant B is about 1.7 times smaller as determined by the present work. The reason for this discrepancy is not clear. One possibility is the fact that the sample used by Bogardus was G. E. Type 102 fused quartz, whereas the sample used in the present work was G. E. Type 151 fused silica. Fused quartz and fused silica differ in the method by which they are produced. Fused quartz is cast from a melt of crushed crystalline quartz, whereas fused silica is formed by a chemical vapor deposition process. Type 151 fused silica is of high chemical quality, has very low residual internal stress, and is homogeneously amorphous. Type 102 fused quartz is of lower chemical quality, may have relatively high residual internal stress, and may contain small quartz crystallites embedded in the amorphous matrix. Whether or not these differences can account for the discrepancy in B, however, can only be resolved by a more systematic investigation.

The relative fit of $\Gamma(a; \delta)$ to the data for the two pure-mode cases in the (001) plane in NaCl was also carried out by use of the general computer program mentioned above. The graphical results are shown in Figs. 7 and 8 for $L(\omega_1)$ propagating,

TABLE IV. Values of the third-order constants A and B from present work and from Bogardus in units of 10^{11} dyn/cm^2 for fused SiO_2.

	A	B
Present	− 5.27 ± 0.30	+5.42 ± 0.33
Bogardus	−4.4 ± 1.2	+9.3 ± 0.8

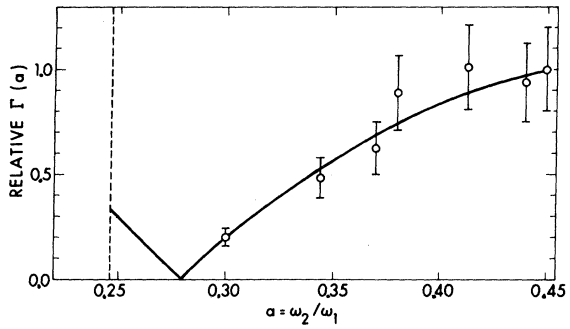

FIG. 7. Best relative fit of $\Gamma(a;\delta)$ to the experimental data (open circles) for the (001) mixing plane and with $L(\omega_1)$ propagating down the [100] axis for NaCl.

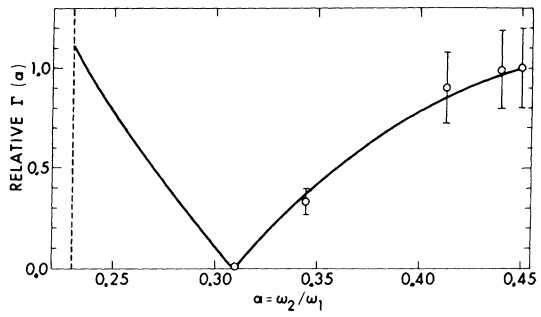

FIG. 8. Best relative fit of $\Gamma(a;\delta)$ to the experimental data (open circles) for the (001) mixing plane and with $L(\omega_1)$ propagating down the [110] axis for NaCl.

respectively, down the [100] and [110] axes. The conversion parameter δ, determined for each case from the best relative fit, is given in Table V, along with values calculated from the data of Chang[11] and Swartz.[12] As was pointed out by Huntington,[13] there are large discrepancies in the three small third-order elastic constants C_{123}, C_{144}, and C_{456}, as reported by Swartz and Chang. These discrepancies are reflected in the value calculated for δ in each case, as can be seen in Table V. It is curious to note that the values of δ determined presently fall very close to the means of the values calculated from the data of Swartz and Chang. This is probably coincidental. As a result, the present measurements lend no preferential support to either Swartz or Chang.

VI. SUMMARY AND CONCLUSIONS

The mixing process $L(\omega_1) - T(\omega_2) \rightarrow T(\omega_1 - \omega_2)$ was studied in fused silica and for the two pure-mode cases in NaCl that occur in the (001) plane. The conversion efficiency for these cases was measured. The third-order elastic constants A and B were determined for fused silica from the best fit of theory to the experimental data. The value for A in the case of fused silica is in good agreement with that measured by Bogardus, but the constant B from the present work is a factor of 1.7 times smaller than that reported by him. In the case of NaCl, the conversion parameter δ was obtained from the best relative fit of the conversion efficiency to the experimental data. The values of δ determined presently lend preferential support to neither Swartz nor Chang. This is due to the error intervals occurring in the data and the fact that the present values fall close to the mean of the values determined from Swartz's and Chang's data, respectively.

The zero in the conversion efficiency for the pure-mode case in the (001) plane with $L(\omega_1)$ propagating down the [110] axis was well determined, yielding good precision in the value of δ. This indicates that the technique can yield precise results if a zero in the conversion efficiency occurs well within the measurable range of input frequency ratio.

ACKNOWLEDGMENTS

The authors would like to extend their appreciation to Dr. Samuel Katz for the use of his ultrasonic equipment. Futhermore, thanks are due to Dr. J. Lawrence Katz for the use of the x-ray equipment in the crystallographic laboratory and to Karl Dunn for advice and programming for data analysis.

TABLE V. Experimental values of the conversion parameter δ, as determined presently and calculated from the data of Swartz and Chang. The mixing plane is the (001) plane.

$L(\omega_1)$ Propagation direction	Present	Chang	Swartz
[100]	-2.85 ± 0.73	-3.29 ± 0.33	-2.185 ± 0.555
[110]	-0.5803 ± 0.0025	-0.496 ± 0.046	-0.6615 ± 0.1275

†Paper based on a dissertation submitted by R. W. Dunham to the faculty of the Department of Physics and Astronomy, Rensselaer Polytechnic Institute, Troy, N. Y., in partial fulfillment of the requirements for a Ph. D. degree.

*Work supported in part by the National Aeronautics and Space Administration and in part by the National Science Foundation.

‡Present address: Navy Underwater Sound Laboratory, New London, Conn. 06320.

[1]F. R. Rollins, Jr., L. H. Taylor, and P. H. Todd, Jr., Phys. Rev. 136, A597 (1964).

[2]V. A. Krasilnikov and L. K. Zarembo, IEEE Trans. Sonics Ultrasonics SU-14, 12 (1967).

[3]G. L. Jones and D. R. Kobett, J. Acoust. Soc. Am. 35, 5 (1963).

[4]L. H. Taylor and F. R. Rollins, Jr., Phys. Rev. 136, A591 (1964).

[5]H. H. Barrett and J. H. Matsinger, Phys. Rev. 154, 877 (1967).

[6]F. Birch, Phys. Rev. 71, 809 (1947).

[7]K. Brugger, Phys. Rev. 133, A1611 (1964).

[8]For further details in the treatment given here, see R. W. Dunham, Ph. D. thesis, Rensselaer Polytechnic Institute, 1969 (unpublished).

[9]F. Grard, Nucl. Instr. Methods 34, 242 (1965).

[10]E. H. Bogardus, J. Appl. Phys. 36, 2504 (1965).

[11]Z. P. Chang, Phys. Rev. 140, A1788 (1965).

[12]K. Swartz, J. Acoust. Soc. Am. 41, 1083 (1967).

[13]H. B. Huntington, Proceedings of the IUPAP International Conference on Science and Technology of Non-Metallic Crystals (unpublished).

PHYSICAL REVIEW B VOLUME 2, NUMBER 4 15 AUGUST 1970

Magnetic Circular Dichroism of the F Band in KF and Quenching of F-Center Spin Polarization by Optical Pumping*

M. P. Fontana

Laboratory of Atomic and Solid State Physics, Cornell University, Ithaca, New York 14850

(Received 27 January 1970)

The magnetic circular dichroism (MCD) of the F absorption band in KF has been detected. The field and temperature dependence of the MCD signal yielded $g_{orb} \sim 1$ and $\Delta = -3.2 \pm 0.4$ meV for the orbital g factor and spin-orbit splitting of the excited state of the F center. The effect of unpolarized optical pumping on the MCD signal was investigated, with the result that at the maximum power level used ($\sim 10^{15}$ photons/sec) approximately 75% of the signal was quenched. The data have have been interpreted using a simple model involving a small (efficiency $\epsilon \sim 0.01$) spin-memory loss while the F-center electron is in the excited state. The fact that the spin polarization of the F center can be completely quenched if the pumping intensity is high enough is sufficient to explain the absence of a spin-dependent contribution to the magnetic circular polarization of the F-center emission observed by Fontana and Fitchen.

1. INTRODUCTION

Recently, the effect of a magnetic field on the emission of the F center in KF was successfully detected.[1] The effect, a small circular polarization of the emission, was independent of temperature and was assigned to orbital Zeeman mixing in the relaxed excited state. The absence of a contribution due to the spin polarization in the ground state of the F center was peculiar, since for all the alkali halides studied in absorption,[2] the paramagnetic contribution to the magnetic circular dichroism (MCD) was dominant for $T < 4.2$ °K. Also, in the case of KCl, the F electron has been shown[3,4] to preserve spin memory during an optical pumping cycle with an efficiency better than 95%. On the other hand, there is a small spin-memory loss during a pumping cycle, and the light levels used to excite the F luminescence in KF were sufficiently high ($> 2 \times 10^{15}$ photons/sec) to expect that any given F center would undergo many optical cycles in a time short compared with the spin-lattice relaxation time. In fact, Schmid and Zimmerman[3] have already shown qualitatively for the F center in KCl that optical pumping can destroy up to 95% of the EPR signal due to spin polarization of the ground state. This spin polarization can also be observed by monitoring the paramagnetic component of the MCD of the F absorption band to which it gives rise.[4]

We have used this latter method to study the effect of optical pumping with unpolarized light on the spin polarization of the ground state of the F center in KF.

Since data on the MCD of the F band in KF are not available in the literature, we first detected and determined the basic properties of the MCD of

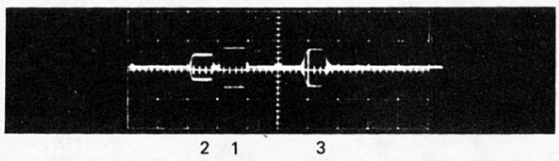

FIG. 5. Display of two impressed rf pulses and resulting rf interaction signal. Horizontal scale: 10 μsec/cm. Vertical scale: Arbitrary.